Journal of
Mechanics of
Materials and Structures

MACROSCALE MODELLING OF MICROSTRUCTURE DAMAGE EVOLUTION BY A RIGID BODY AND SPRING MODEL

Siro Casolo

Volume 4, Nº 3 March 2009

mathematical sciences publishers

JOURNAL OF MECHANICS OF MATERIALS AND STRUCTURES
Vol. 4, No. 3, 2009

MACROSCALE MODELLING OF MICROSTRUCTURE DAMAGE EVOLUTION BY A RIGID BODY AND SPRING MODEL

SIRO CASOLO

A mechanistic approach is presented for macroscale modelling of a structured solid material. The model consists of an assemblage of rigid mass-elements connected to each other by normal and shear line-springs at each side. The characteristics of these springs govern the macroscopic behaviour of the model that is able to incorporate an internal length and a polarity, in analogy with an orthotropic Cosserat solid material. The present numerical implementation addresses the in-plane modelling of a masonry-like composite whose main macroscopic constitutive aspects are: very low tensile strength, texture-dependent evolution of the damage, and orthotropy of shear strength and internal friction. The constitutive rules are assigned by following a heuristic approach, based on the main in-plane damage mechanisms that are identified at the mesoscale, on a representative volume element of the composite solid material. In particular, specific separate constitutive laws for the normal and the shear springs are adopted. Two numerical tests compare the present macroscale approach with a detailed finite element micromodelling, and demonstrate the capability of the proposed model to describe the main microstructure features of the damaging process with very few degrees of freedom.

1. Introduction

The mechanical response and damage evolution of a composite material made with a periodic texture are strictly related to its internal geometry and to the ratio between the microstructure characteristic length and the global size of the system. In the present study, attention is focused on the postelastic macroscale response of a plane masonry-like material that is composed of blocks jointed by mortar layers where the strain tends to localise and the main part of the mechanical degradation occurs. It is well known that the texture geometry produces perceivable effects at the macroscale that tend to evolve and to become more evident with the progressive degradation of the material. In particular, the different topology of the continuous horizontal mortar joints with respect to the vertical joints, interrupted by the blocks, causes a marked orthotropy of the macroscopic shear response, as also shown by specific laboratory experiment [Malyszko 2005].

Experiments as well as numerical and analytical studies have shown that often the damage behaviour of a masonry-like material can be described on the basis of a limited number of mesoscale mechanisms [Dhanasekar et al. 1985; Zucchini and Lourénço 2002]. At the macroscale level, most of these damage mechanisms can be modelled in the frame of a Cauchy solid continuum approach [Lourénço et al. 1997; Pietruszczak and Ushaksaraei 2003; Massart et al. 2004; Milani et al. 2006]. Nevertheless, there are cases in which microscale effects need to be explicitly considered and the description of the mechanical degradation entails taking into account the local rotation of the blocks and the orthotropy of shear

Keywords: RBSM, rigid, spring, macroscale, microstructure, heuristic, Cosserat.

strength. Dealing with regular textures, the micro/macroscale transition can thus be performed toward an enriched generalised continuum, which retains some information on the microstructure and internal length [Masiani et al. 1995; Sulem and Mühlhaus 1997; Forest and Sab 1998]. More recently, the relationship between the micro and macroscale for the specific case of masonry-like periodic rigid block assemblies has also been handled by resorting to a multiscale strategy [Trovalusci and Masiani 2005; Brasile et al. 2007].

An alternative computational approach that adopts a specific *mechanistic* model was proposed in [Casolo 2004]. In this case, the heterogeneous solid material is imaged as a mechanism consisting of rigid masses connected by simple elastic-plastic damaging springs, in the spirit of the rigid body spring model (RBSM) [Kawai 1978; Griffiths and Mustoe 2001; Ostoja-Starzewski 2002] and somewhat in the vast family of discrete element models [Lemos 2007]. Given a representative volume of the periodic heterogenous solid material, the core of the proposed model is a macroscopic mechanical device consisting of 4 masses connected by springs, as shown in Figure 1. This discrete mechanical device should possess the relevant macroscopic properties of the periodic microstructured solid material, and we tentatively name it the *representative macroscopic segment* or *heuristic molecule*. The linear elastic characteristics of the three line springs that connect the elements at each side can be defined either by the relationship with a corresponding continuum or by a direct computational approach [Casolo 2006]. To describe the mean damage evolution of the material, a heuristic approach was initially proposed in [Boffi and Casolo 1998], and then in [Casolo and Peña 2007], based on the phenomenological consideration of the main in-plane damage mechanisms that can be described at the mesoscale.

The sequel of such research is presented in this paper, with the emphasis now placed on discerning the impact of material texture on the orthotropic damage evolution at the macroscale level. As a case study, a masonry-like material made of three material components is considered: the blocks, and the horizontal and vertical mortar joints. The load is applied on an area whose size is comparable with the internal microstructure length of the periodic arrangement. In this case the orthotropy of the shear response and the local rotation of the blocks play an important role in the development of damage, also at the

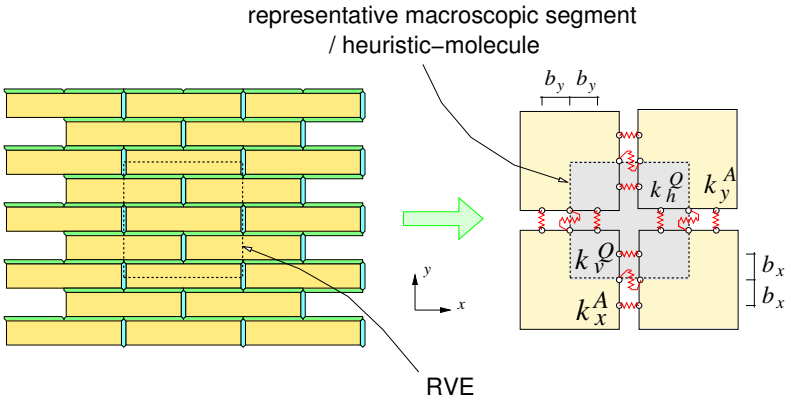

Figure 1. Heuristic representation of the correspondence between an RVE (representative volume element) of the composite material and the representative macroscopic segment, or heuristic molecule, made of rigid masses and springs.

macroscale. The numerical application presented at the end of the paper will investigate and compare the proposed mechanistic model with a finite element continuum model that describes the masonry-like texture with a microscale level of detail, assuming a modified Drucker–Prager plasticity model for the three material components [ABAQUS 2007].

2. The macroscale rigid body and spring model

2.1. ***Discrete formulation of the kinematics.*** The masonry-like composite material is modelled as a plane solid body partitioned into m quadrilateral mass-elements ω^i such that no vertex of one quadrilateral lies on the edge of another quadrilateral [Casolo 2006]. Given a global reference frame $\{O, x, y\}$, the deformed configuration of the discrete model is described by the displacements and rotation $\{u_i, v_i, \psi_i\}$ of the local reference frames $\{o^i, \xi^i, \eta^i\}$ fixed in each element's barycentre o^i. These $3m$ variables are assembled into the vector of Lagrangian coordinates $\{u\}$ that is conjugated in virtual work with the corresponding vector of external loads $\{p\}$ (see Figure 2a), as

$$\{u\}^T = \{u_1, v_1, \psi_1, u_2, v_2, \psi_2, \ldots, u_m, v_m, \psi_m\}, \qquad \{p\}^T = \{p_1, q_1, \mu_1, p_2, q_2, \mu_2, \ldots, p_m, q_m, \mu_m\}.$$

Three line springs connect each couple of adjoining mass-elements in correspondence of points P, Q and R, placed along the common side as shown in Figure 2b.[1] Then, average strain measures are associated with these connecting devices: the axial strains, ε^P and ε^R, are associated with the volumes of pertinence V^P and V^R, while the shear strain ε^Q is associated with the volume V^Q, defined by $\mathrm{V}^Q = \mathrm{V}^P + \mathrm{V}^R$. Considering a discrete model with r sides that connect all the elements, the generalised strain vector $\{\varepsilon\}$ and the diagonal matrix of volumes of pertinence $[V]$ are defined as

$$\begin{aligned} \{\varepsilon\}^T &= \{\varepsilon_1^P, \varepsilon_1^Q, \varepsilon_1^R, \varepsilon_2^P, \varepsilon_2^Q, \varepsilon_2^R, \ldots, \varepsilon_r^P, \varepsilon_r^Q, \varepsilon_r^R\}, \\ [V] &= \operatorname{diag}\{\mathrm{V}_1^P, \mathrm{V}_1^Q, \mathrm{V}_1^R, \mathrm{V}_2^P, \mathrm{V}_2^Q, \mathrm{V}_2^R, \ldots, \mathrm{V}_r^P, \mathrm{V}_r^Q, \mathrm{V}_r^R\}. \end{aligned} \tag{1}$$

Under the assumption of small displacements, the strain-displacement relation can be expressed by considering a $3r \times 3m$ matrix $[B]$ as $\{\varepsilon\} = [B]\{u\}$ (see Appendix A for a specific example).

2.2. ***Incremental formulation of the balance laws.*** A measure of stress, conjugated in virtual work with the strain associated to each connecting device, is introduced, and the corresponding vector of generalised stress $\{\sigma\}$ is assembled as $\{\sigma\}^T = \{\sigma_1^P, \sigma_1^Q, \sigma_1^R, \sigma_2^P, \sigma_2^Q, \sigma_2^R, \ldots, \sigma_r^P, \sigma_r^Q, \sigma_r^R\}$. Out of the linear elastic field, the stress σ and the tangent stiffness k of each spring depend on the whole past deformation history (designated by the symbol $\star$) which is subdivided into discrete time intervals. Given the stress σ^0 for a generic spring at instant t_i, the following linear expression is adopted for predicting the stress at instant $t \in [t_i, t_{i+1}]$: $\sigma(t, \star) = \sigma^0(t_i, \star) + k(t_i, \star)\Delta\varepsilon$, with $\Delta\varepsilon$ being the evaluated strain increment in the spring. The *local* tangent stiffness matrix $[D_t]$ of all the connecting springs is

$$[D_t] = \operatorname{diag}\{k_1^P, k_1^Q, k_1^R, k_2^P, k_2^Q, k_2^R, \ldots, k_r^P, k_r^Q, k_r^R\}. \tag{2}$$

[1]The absence of the axial springs that connect the rigid elements along the diagonals of the heuristic molecule limits the present RBSM to behaving at the macroscale like a solid material with a Poisson's ratio of zero. This has been assumed for simplicity, after considering the limited importance of the Poisson effect for the main damaging mechanisms of a masonry-like composite material. In general, a range of different values for the macroscopic Poisson's coefficient can be obtained by combining different types of spring (axial, shear, or rotational) and by an appropriate definition of the lattice geometry [Stakgold 1950; Ostoja-Starzewski 2002].

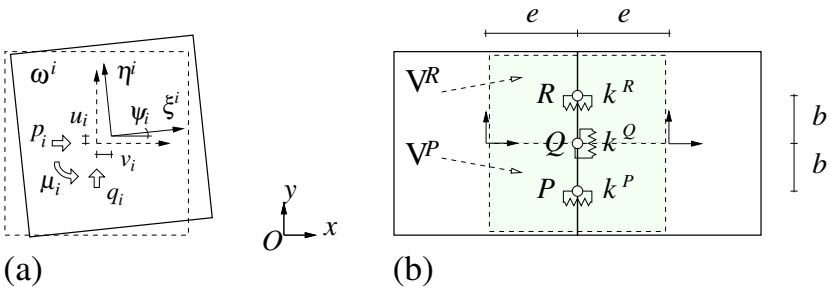

Figure 2. Notation adopted and disposition of the connecting springs [Casolo and Peña 2007].

Thus, the internal virtual work done by the elastic-plastic springs is

$$\delta\mathcal{W}^i = \{\delta\varepsilon\}^T[V]\{\sigma^0\} + \{\delta\varepsilon\}^T[V][D_t]\{\Delta\varepsilon\} = \{\delta u\}^T(\{f^0\} + [K_t]\{\Delta u\}), \tag{3}$$

where $\{f^0\}$ is the vector of generalised forces and $[K_t]$ is the generalised tangent stiffness matrix, defined as $\{f^0\}^T = \{\sigma^0\}^T[V][B]$, and $[K_t] = [B]^T[V][D_t][B]$, respectively. On the other hand, the virtual work done by the external forces is simply $\delta\mathcal{W}^e = \{\delta u\}^T\{p\}$. Then, by means of the balance of virtual works $\delta\mathcal{W}^i = \delta\mathcal{W}^e$, $\forall\{\delta u\}$, the following system of incremental static equations is obtained:

$$\{f^0\} + [K_t]\{\Delta u\} = \{p\}. \tag{4}$$

This is solved adopting the full Newton–Raphson iteration scheme until numerical convergence is attained [Zienkiewicz and Taylor 1991].

2.3. ***Constitutive laws: linear elastic field.*** A computational approach based on the five elemental loading tests sketched in Figure 3 is adopted, in the linear elastic field, to identify the four spring stiffness k_x^P, k_y^P, k_x^Q, and k_y^Q, and the two distances b_x and b_y [Casolo 2004]. Alternatively, these six parameters can also be obtained by a direct relation with the elastic tensor C of an "equivalent" orthotropic

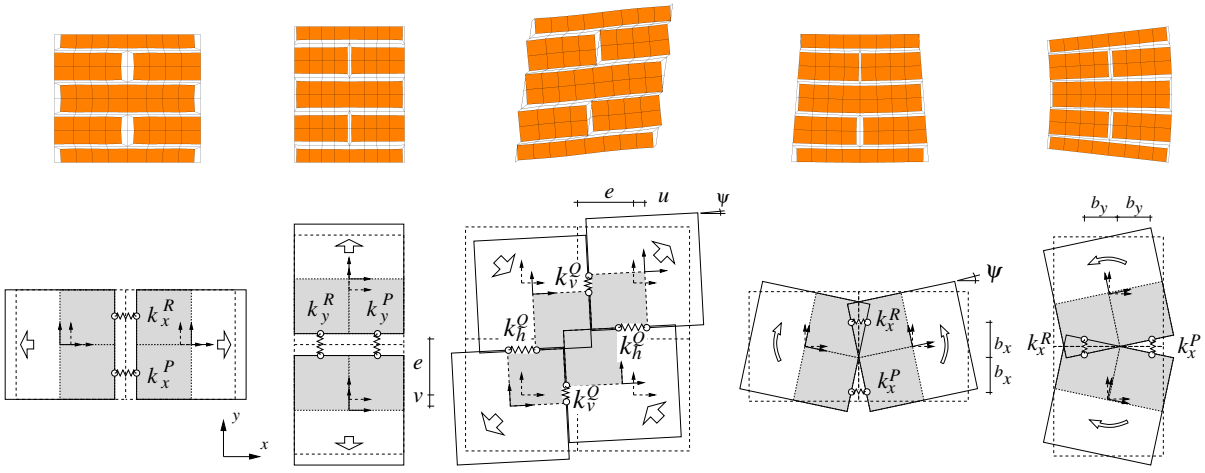

Figure 3. Scheme of the deformed shape of the five elemental tests of loading. The finite element model of the RVE (top row) and the the corresponding rigid element schemes (bottom row).

Cosserat continuum,[2] as explained in [Casolo 2006] and summarised in Appendix B. The microscale model adopts a very common masonry-like texture, with a typical Italian brick geometry for the blocks: $2l \times 2h = 25 \times 5.5\,\text{cm}$. The case of single leaf masonry is considered here for the sake of clarity as a first approach, with a depth of 12 cm. The reference RVE is a $26 \times 26\,\text{cm}$ square domain made by finite elements. Homogeneity, isotropy, and perfect bonding are assumed for the three components of the heterogeneous masonry-like material. The elastic modulus of the blocks is $E_b = 10000\,\text{MPa}$, the elastic moduli of the horizontal and the vertical mortal joints are $E_h = 2000\,\text{MPa}$ and $E_v = 1000\,\text{MPa}$, respectively, while the Poisson's coefficient is fixed as $\nu = 0.1$ for all the components.

The stiffness of the axial springs can be directly computed by considering the RVE subjected to simple normal loading acting parallel to a material principal direction and traction-free boundary condition along the other two sides (the first and second loading cases, in the left part of Figure 3). Given the generalised axial strains $\varepsilon_x = u/e$ and $\varepsilon_y = v/e$, and the corresponding average elastic energy densities $\mathcal{U}_x^A$ and $\mathcal{U}_y^A$, then the axial stiffnesses per unit volume to be attributed to the normal connecting devices are

$$k_x^P = \frac{2\mathcal{U}_x^A}{\varepsilon_x^2}, \qquad k_y^P = \frac{2\mathcal{U}_y^A}{\varepsilon_y^2}. \tag{5}$$

The evaluation of the shear response requires some more attention. In fact, in addition to the mean shear deformation E_s it is necessary to select a criterion for measuring the mean local rotation ψ of the blocks [Casolo 2006]. A direct test can be made, in which the RVE is subjected to periodic displacement boundary conditions and loaded by shear actions along the four boundaries that have equal absolute value $S_{12} = S_{21}$ (this is the loading case shown in the centre of Figure 3). The average symmetric shear strain is $\varepsilon_s = (u + v)/2e$, while the average local rotation measured on the blocks is directly assigned to the rigid elements. The generalised shear strains for the vertical and the horizontal connecting devices are then

$$\varepsilon_v = \varepsilon_s - \psi = \varepsilon_s(1 - \rho), \qquad \varepsilon_h = \varepsilon_s + \psi = \varepsilon_s(1 + \rho), \tag{6}$$

with the local rigid rotation ratio $\rho = \psi/\varepsilon_s$. The equilibrium of the shear stresses implies that the stiffnesses of the shear connecting devices of the vertical and horizontal sides must be related by the following equation:

$$\frac{k_h^Q}{k_v^Q} = \frac{\varepsilon_v}{\varepsilon_h} = \frac{1 - \rho}{1 + \rho}. \tag{7}$$

Thus, a generalized symmetric shear stiffness k_s can be defined, such as

$$k_v^Q = (1 + \rho)k_s, \qquad k_h^Q = (1 - \rho)k_s.$$

Finally, k_s is defined as a function of the average elastic energy $\mathcal{U}_s$ per unit volume stored in the volume of pertinence:

$$k_s = \frac{\mathcal{U}_s}{(1 - \rho^2)\varepsilon_s^2} \tag{8}$$

[2]Clearly, the reduction from eight to six parameters in the passage from the plane orthotropic Cosserat continuum to the present RBSM implies a loss of information about the axial and shear coupling effects. The correspondence would be ideal in the case of an equivalent Cosserat continuum with a *diagonal* elastic tensor as proposed in [Masiani et al. 1995; Sulem and Mühlhaus 1997].

The distances b_x and b_y of the axial springs from the mid-point of each side are evaluated by means of the two in-plane bending tests, shown in Figure 3 on the right. After measuring the average elastic energy densities $\mathcal{U}_x^F$ and $\mathcal{U}_y^F$ from the RVE finite element model, we have

$$\beta_x = \frac{b_x}{e} = \frac{1}{\psi}\sqrt{\frac{2\mathcal{U}_x^F}{k_x^P}}, \qquad \beta_y = \frac{b_y}{e} = \frac{1}{\psi}\sqrt{\frac{2\mathcal{U}_y^F}{k_y^P}}. \tag{9}$$

The six values identified for the springs in the linear-elastic field are as follows:[3]

$$\begin{aligned} k_x^P &= 5650\,\text{MPa} \qquad k_h^Q = 3520\,\text{MPa} \qquad \beta_x = 0.61 \\ k_y^P &= 7600\,\text{MPa} \qquad k_v^Q = 11780\,\text{MPa} \qquad \beta_y = 0.57 \end{aligned} \tag{10}$$

2.4. *Constitutive laws: elastic-plastic field.*

2.4.1. *Overview of the heuristic approach.* Modelling the mechanical degradation when the effects at the microstructure level entail taking the local rotation of the blocks and the orthotropy of shear strength into account is the focus of this contribution. To do this, the main hypothesis of the proposed constitutive model is that the damage evolution can be described using a limited number of mesoscale mechanisms that are strictly related with the internal microstructure geometry [Malyszko 2005; Trovalusci and Masiani 2005].

The five basic mesoscale elemental mechanisms are sketched in Figure 4:

(i) cracking of vertical joints with sliding of bed-joint under horizontal tension;

(ii) global crushing and local splitting of joints under horizontal compression;

(iii) bed-joints cracking and opening under vertical tension;

(iv) global crushing given by simultaneous splitting of blocks and cracking of vertical joints under vertical compression; and

(v) shear sliding of mortar joints along a stepwise pattern under shear loading with *local* rotation of the blocks.

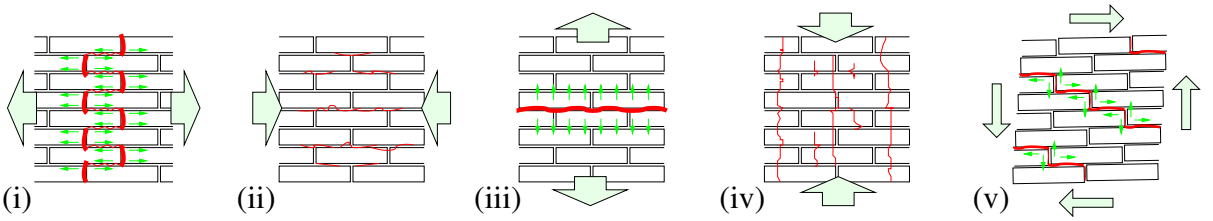

Figure 4. Heuristic description of the five types of damage mechanism considered at the mesoscale.

[3]Note that the size effect can significantly affect the macroscopic response of microstructured materials. Ideally, when the size of the discrete elements is much larger than the characteristic length of the RVE, then the parameters that govern the microstructure effects must become negligible at the macroscale level. The present RBSM is designed to deal with this aspect by progressively reducing the orthotropy of the shear springs and by making β_x and β_y tend to $1/\sqrt{3}$, as described in [Casolo 2004].

Mechanisms (i) and (v) are those for which the effect of the texture on the global response is more significant. In fact, in the first case the tensile strength is strictly related to the aspect ratio of the blocks, in combination with the friction coefficient of the horizontal mortar joints and the presence of a vertical compressive stress. On the other hand, in the last mechanism the mean local rotation of the blocks as well as the orthotropy of the shear response is also strictly related to the shape and disposition of the blocks. Moreover, it is evident that the presence of a mean compression stress has an impact on the strength characteristics that is orthotropic and depends on the texture geometry.

The proposed constitutive model exploits the observation that the mesoscale damage mechanisms are limited, by associating a particular damage pattern almost exclusively to each type of spring. The model works at the macroscale, without the need of describing the effective texture geometry with the mesh; this is the essential difference with respect to the classical continuum approach usually adopted in finite element models, which generally require to describing the geometry of the material microstructure, except when adopting a generalised continuum [Masiani et al. 1995]. Clearly, in the present formulation the springs should be as much as possible aligned with the principal axes of the material texture, otherwise a good approximation cannot be taken for granted. Furthermore, at present no particular steps have been taken to deal with the localisation and the mesh objectivity which are a consequence of strain-softening material behaviour [Lourénço et al. 1997; de Borst 2001]. As a rule of thumb, the model should be composed by units whose size is approximately comparable to the size of the RVE. In any case, the tests presented in the following section will reveal a limited sensitivity with respect to mesh size.

Even if the present work is focused on the monotonic response, this notwithstanding the RBSM is implemented into a computer code that is designed to perform dynamic analyses. Thus, the constitutive laws also include the hysteretic response, with different rules for strength and stiffness degradation of the axial and shear springs, as is schematically shown in Figure 5, by following the paths indicated by the points labelled 1–9. The skeleton curves degrade depending on the maximum positive and maximum negative deformation reached during the loading history. The degradation of loading stiffness, unloading stiffness, and strength also depends on the maximum deformation reached. Out of the range of deformation defined by the interval $[S^-, S^+]$, the skeleton curves are horizontal and correspond to a residual strength which is assumed to remain constant until the ultimate deformation is reached. These hysteretic rules are strictly derived from those already described with more detail in [Casolo 2000; Casolo and Peña 2007], based on phenomenological evidence [Naraine and Sinha 1991; Binda et al. 1992; Magenes

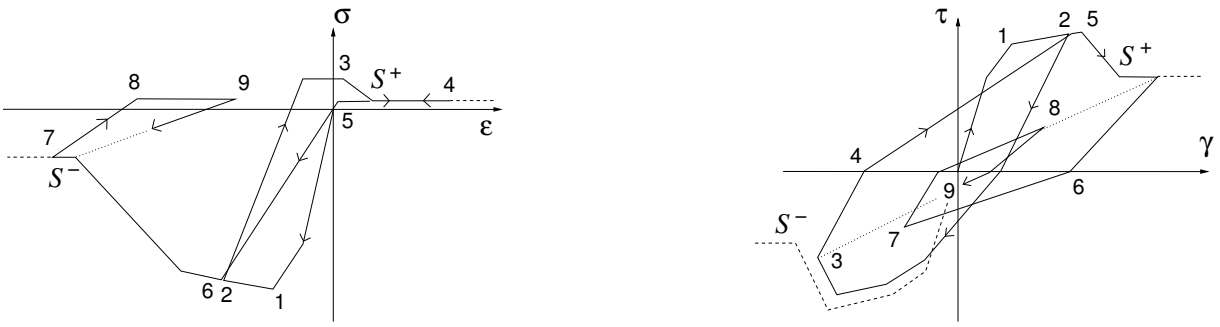

Figure 5. Hysteretic behaviour of the axial (left) and shear (right) connecting springs.

	$p_t\|_0$ (MPa)	ϕ (°)	ϑ (°)
Brick	0.425	30	5
Horizontal mortar	0.10	30	5
Vertical mortar	0.05	30	5

Table 1. Parameters assigned to the material components of the masonry-like RVE: $p_t|_0$ is the initial hydrostatic tension strength of the material, while ϕ and ϑ are the material angle of friction and the dilatation angle, respectively.

and Calvi 1992; Anthoine et al. 1995], while in the following sections attention will be only devoted to define the parameters that govern the monotonic response.

2.4.2. *Monotonic tests on the finite element RVE.* The RVE is made by 4-node bilinear generalised plane strain finite elements that adopt the Drucker–Prager plasticity material model available within [ABAQUS 2007]. The hyperbolic yield criterion has been assigned to the three material components: the bricks, and the horizontal and vertical mortar joints. This criterion is a continuous combination of the maximum tensile stress condition of Rankine (tensile cut-off) and the linear Drucker–Prager condition at high confining stress:

$$F = \sqrt{\left(d'|_0 - p_t|_0 \tan\phi\right)^2 + q^2} - p\tan\phi - d' = 0, \tag{11}$$

where d' is the hardening parameter, $p_t|_0$ is the initial hydrostatic tension strength of the material, ϕ is the material angle of friction, q is the von Mises equivalent stress, and p is the equivalent pressure stress.[4] In the present application, the hardening parameter is

$$d' = \sqrt{(d'|_0 - p_t|_0 \tan\phi)^2 + d^2}, \tag{12}$$

and it is defined by the cohesion yield stress, $d = \sqrt{3}\tau$, data (where τ is the yield stress in a shear test) as a function of the equivalent shear plastic strain

$$\overline{\varepsilon}^{pl} = \frac{\gamma^{pl}}{\sqrt{3}}.$$

The values assigned to $p_t|_0$, ϕ, and the dilatation angle ϑ in the $p-q$ plane at high confining pressure are reported in Table 1, while the hardening behaviour of the three elemental materials is shown in Figure 6, left, in terms of a simple shear test.[5] The finite element mesh of the composite RVE is shown in Figure 6, right. The thickness of the mortar joints is $t = 1$ cm, and the vertical head-joints, interrupted by the bricks, are considered as weaker than the horizontal continuous bed-joints.

[4] In more detail, according with the notation of the [ABAQUS 2007] manual, $p = -\frac{1}{3}\,\mathrm{tr}\,[S]$ and $q = \sqrt{\frac{2}{3}[S^d] : [S^d]}$, where $[S]$ is the Cauchy stress tensor.

[5] The flow potential is $G = \sqrt{(0.1d|_0 \tan\vartheta)^2 + q^2} - p\tan\vartheta$, with $d|_0$ the initial cohesion yield stress. This flow potential is continuous and smooth and ensures that the flow direction is always uniquely defined. This function approaches the linear Drucker–Prager flow potential asymptotically at high confining pressure stress and intersects the hydrostatic pressure axis at 90° [ABAQUS 2007].

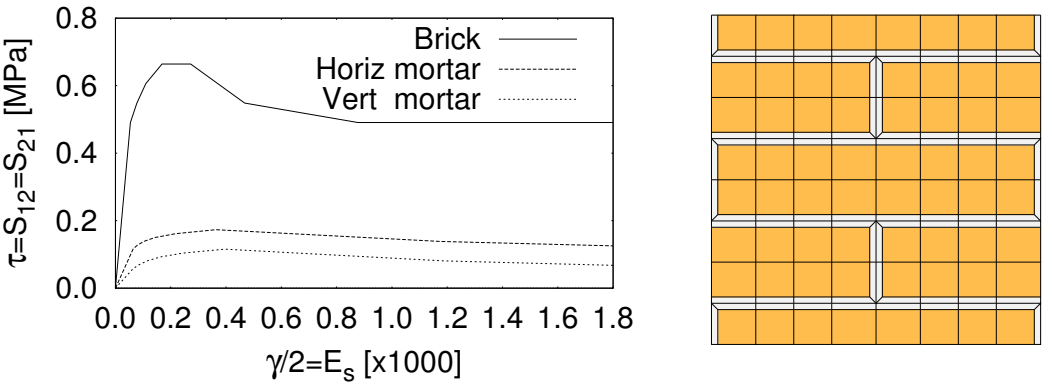

Figure 6. Left: Hardening behaviour in a shear test for the three elemental materials. Right: Finite element mesh of the RVE.

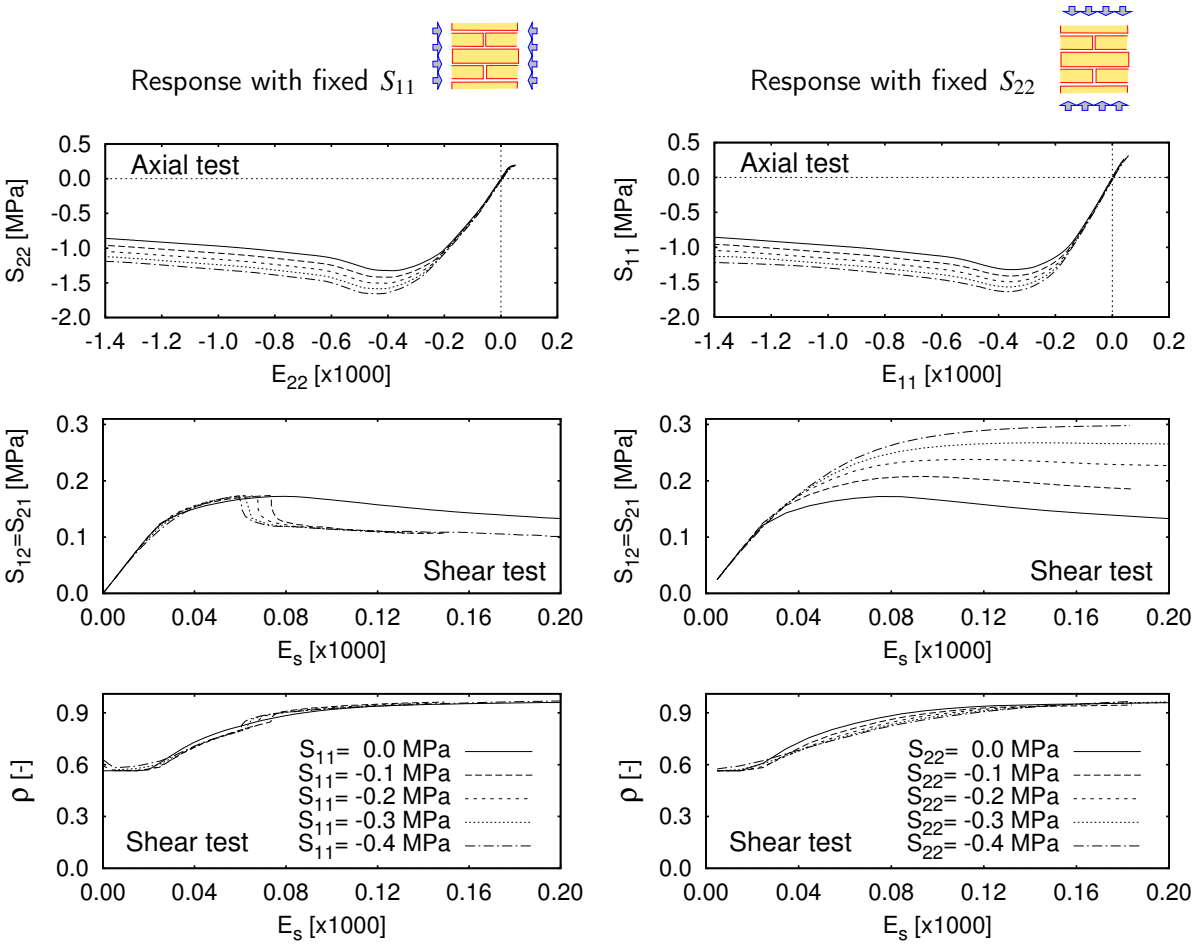

Figure 7. Macroscale results of the monotonic tests on the finite element RVE.

Four sets of elemental computational tests were considered on the basis of the heuristic description already sketched in Figure 4. At the macroscale, the effect of the internal friction is evaluated by considering tests with a different level of mean compression along the horizontal and vertical principal directions. The responses, written in terms of mean stress-strain relations, are reported in detail in Figure 7. The following synthetic observations can be made:

- *Tension*: In this case the strength is very low and the calculated response appears to be completely brittle due to the lack of numerical convergence of the computer code. Note that the strength along the horizontal direction (top right) is higher than along the vertical direction (top left) because the vertical joints are interrupted by the blocks.
- *Compression*: In this case the material exhibits its maximum bearing capacity with a progressive mechanical degradation once the peak value of the strength is reached. In the present case the response is almost isotropic.
- *Shear*: This case is governed by the response of the mortar joints. The residual shear strength is enhanced by a vertical compression, obeying a Coulomb-type relation, while the presence of a horizontal mean compression produces a global instability.
- *Local rotation*: In the case of symmetric shear loading the texture effects are evident, involving the local rotation of the blocks, measured by the angle ψ. The ratio $\rho = \psi/\varepsilon_s$ is reported in Figure 7 as a function of the symmetric shear deformation E_s, where $E_s = (E_{12} + E_{21})/2$.

2.4.3. *Definition of the constitutive laws of the springs.* The elastic-plastic characteristics given to the connecting springs descend from the identification tests made on the RVE, summarized in Figure 7.

In the macroscopic compression region the constitutive laws of the axial springs are directly related to the axial responses of the reference RVE, as shown in the top row of Figure 8, while for simplicity β_x and β_y have the fixed values reported in (10) on page 556. In the tensile region, on the other hand, the completely brittle response of this RVE at the macroscopic level is mainly due to a global lack of numerical convergence of the computer code. In fact, when adopting uneven loading conditions the tensile behaviour exhibits some strain softening at the local level. Unfortunately this effect is not easily quantifiable, since it depends on the size of the specimen as well as on the different boundary conditions. Thus, a softening behaviour has been tentatively given to the axial springs under tensile loading by assigning a negative slope that is in accord with the negative slope of the compression branch, as shown in Figure 8.

The definition of the horizontal and vertical shear springs requires fitting both the macroscale response in terms of the symmetric shear stress-strain relation and the evolution of the local rotation ratio ρ as a function of the mean shear strain $E_s = \varepsilon_s = (\varepsilon_h + \varepsilon_v)/2$. To do this, different constitutive laws are assigned to the vertical and horizontal shear springs, as shown in the middle row of Figure 8, according with the criterion already explained in [Casolo 2004]. A partial validation of the combined effect of these assignments on the global shear behaviour is shown in the bottom row of Figure 8, where the macroscopic responses of the RBSM heuristic molecule in terms of $\tau_s(\varepsilon_s)$ and $\rho_s(\varepsilon_s)$ are compared with the finite element RVE.

Since the macroscale shear strength is enhanced by the presence of vertical compression, it is also assumed that the shear skeleton curve translates as a function of the mean vertical axial stress $\overline{\sigma}_v$ in the

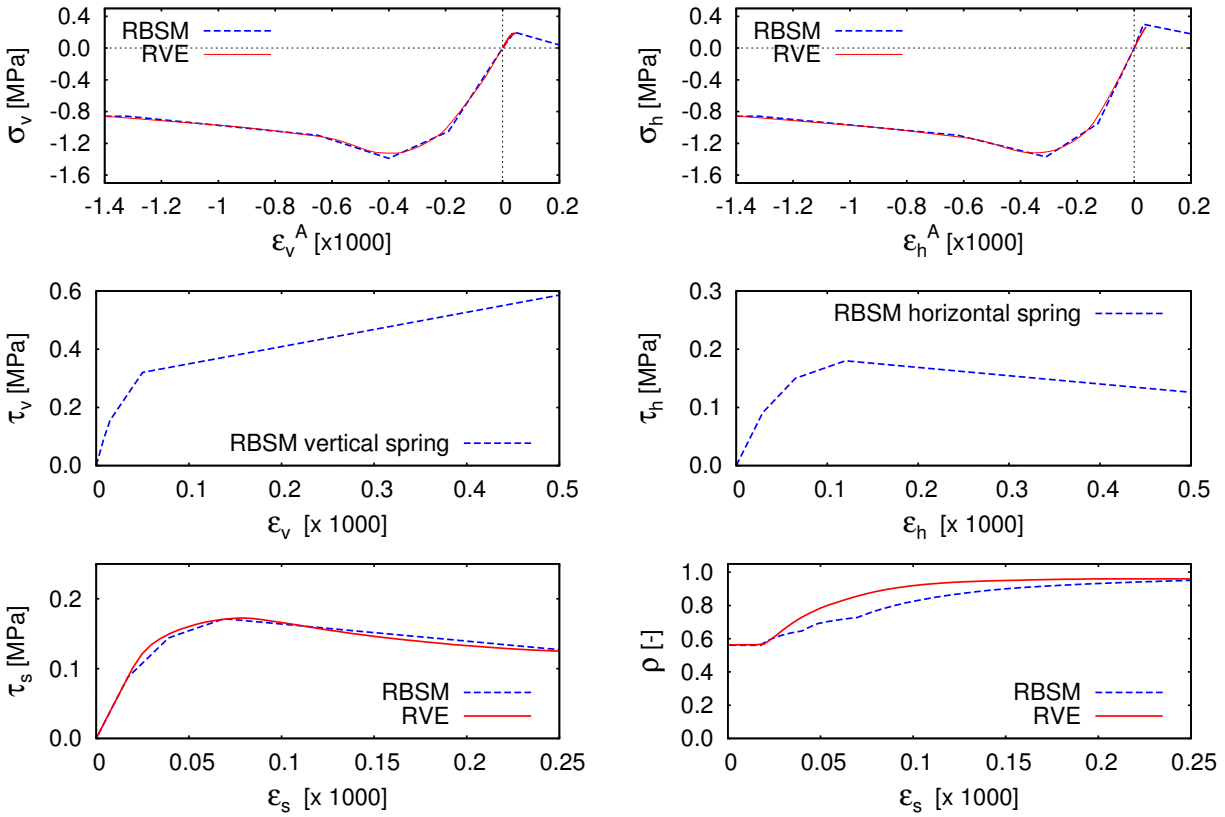

Figure 8. Elastic-plastic characteristics of the rigid element springs. The the characteristics of the axial springs (top row), and the characteristics of the shear springs and the corresponding local rotation ratio ρ (middle and bottom rows).

corresponding volume of pertinence V^Q, as shown in Figure 9. From the results of the shear test with fixed S_{22}, the value $\phi = 0.3$ has been given to this Coulomb-type internal friction coefficient. At present, the model assumes that the influence of the shear on the response of the axial springs is negligible.

Up to now, no specific steps have been taken to deal with localisation and mesh objectivity, which are consequences of strain-softening material behaviour [Lourénço et al. 1997; de Borst 2001].

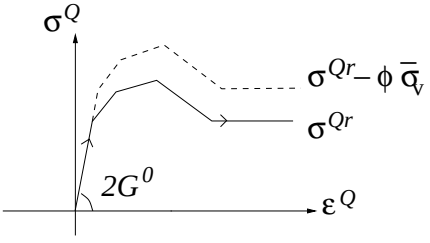

Figure 9. Variation of the skeleton curve of a shear spring as a function of the mean vertical stress $\overline{\sigma}_v$.

3. The case study

To evaluate the performance of the present approach, a situation where the microstructure effects are significant has been investigated in depth. The case study is a square plane domain subjected to two boundary and loading conditions that cause a highly nonhomogeneous stress-strain field, also at the macroscale. The vertical and the horizontal load are monotonically applied over a distributed small volume, as shown in the scheme of Figure 10, left. The parts drawn with dotted line hatching indicate a kinematic boundary condition of full clamping. Note that the block size is not far from the macroscale characteristic length of the problem.

3.1. ***Response of the reference FE wall.*** The microscale model adopted as the reference wall is made by means of a refined mesh of 3600 plane 4-node bilinear finite elements as shown in Figure 10, right, for a total of 7425 degrees of freedom.

Figure 11 shows the maps of the deformed shape and of the equivalent plastic strain (called PEEQ in ABAQUS) for a loading configuration close to the collapse. The response of this FE model clearly reveals the role played by the masonry-like texture that produces quite different kinematics of the two collapse mechanisms. This is due to the combined effect of the texture geometry with the internal friction, that enhances the shear strength of the horizontal joints in the presence of a vertical pressure. In the case of vertical applied load, the collapse mechanism involves a significant local rotation of the blocks, while in the case of horizontal load the kinematics can be mainly described in terms of horizontal relative translation of the blocks. As a first consequence, the distribution of the plastic strain evidences a diffused damaged area in the first case, while the damage is concentrated in few horizontal layers of mortar with the horizontal load. At the macroscale, the final consequence is that we have a very different bearing capacity, with a maximum vertical load that is 83% higher than the maximum horizontal load

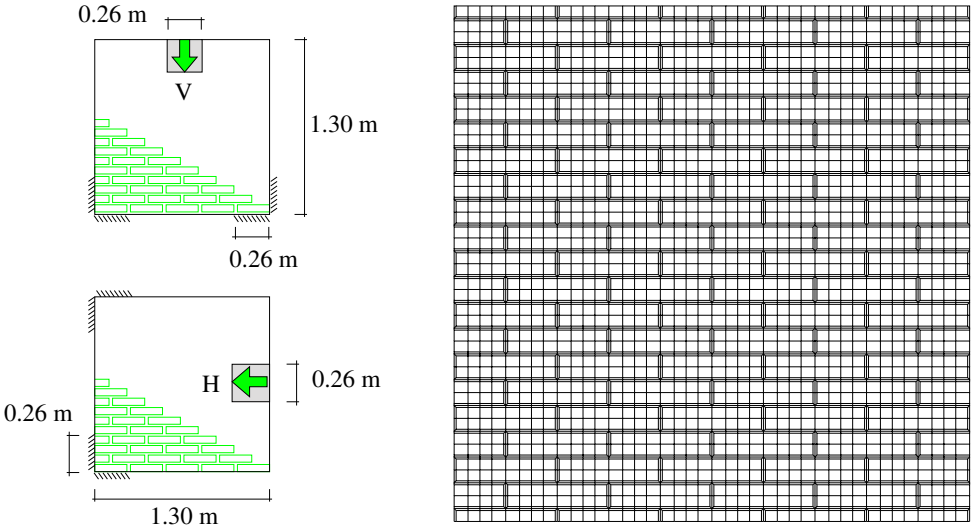

Figure 10. Left: scheme of the masonry walls used as reference. Right: finite element mesh for the microscale reference model.

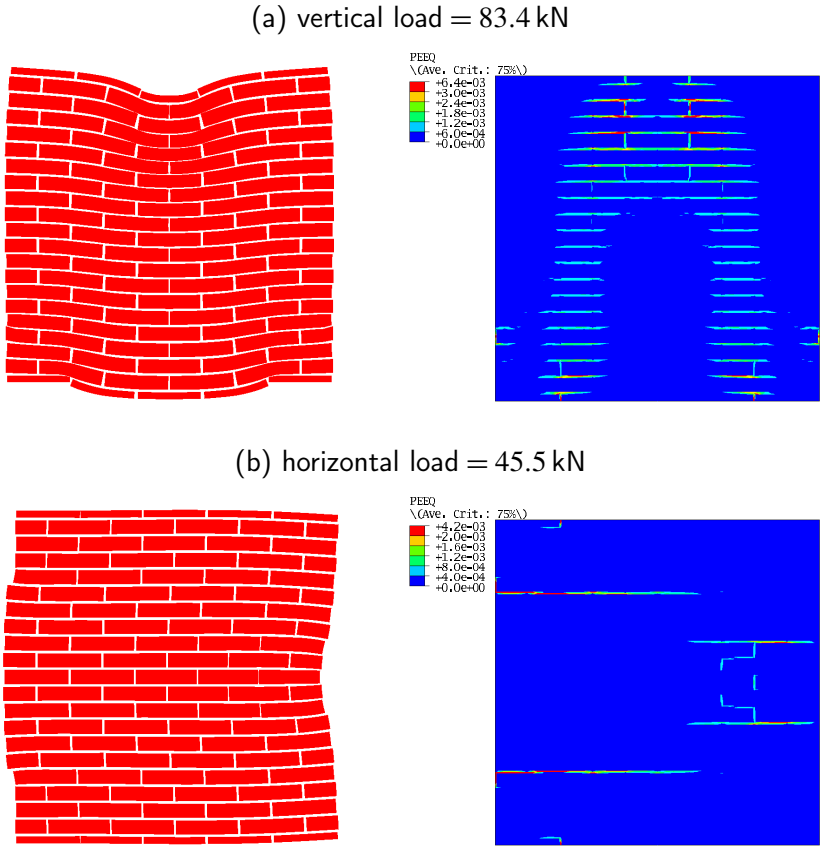

Figure 11. Deformed shape and equivalent plastic strain (peeq) for the microscale finite element model for a configuration close to collapse. The vertical (a) and horizontal (b) applied loads.

(~ 84 kN versus ~ 46 kN).[6] Also quite different is the trend of the decay of the stiffness as a function of the increasing displacement at the point of application of the load.

3.2. ***Response of the RBSM.*** The response of the RBSM is here presented making reference to regular meshes of 5×5, 10×10 and 20×20 square elements (hence 75, 300 and 1200 degrees of freedom). With this model, the fully clamped boundary condition should be intended in the sense that the border elements are connected to a solid base that is completely rigid. Ideally, this base could be also modelled by a rigid body and springs that have infinite stiffness. In practice, the connecting springs placed along the clamped boundary have an effective length that is half that of the internal ones, while the strength remains unchanged.

[6]It is interesting to recall that in the laboratory experiment by Malyszko [2005] the orthotropic shear strengths were evaluated by arranging the boundary conditions as to obtain a predetermined single plane of failure: (i) for a loading H tangential to the bed joints, and (ii) for a loading V normal to the bed joints. In the first case the global strength was related to the shear strength of the horizontal mortar joint, while in the second case the collapse mechanics was more complex and the shear strength of the bricks was also determinant. The ratio of the two shear strengths was $V/H = 1.65$.

First, the capability of the present model to account for the specific microstructure effects can be appreciated from the maps shown in Figure 12, which report the responses of the two RBSMs subjected to the same value of load, equal to 35 kN, along the vertical and horizontal directions. This load produces some mechanical degradation in these models, with a decay of $\sim 10\%$ of the global stiffness in the case of vertical load, and a decay of $\sim 30\%$ in the case of horizontal load. In this test, it is noticeable that the central part of the model subjected to the vertical load presents horizontal stripes of alternate positive and negative axial stress σ_h, which indicates the presence of a *local in-plane* flexural mechanism. Clearly, this effect is strictly related to the specific RBSM capability of retaining memory of the original internal texture. In fact, this behaviour is correctly absent in the case of a horizontal applied load. From these

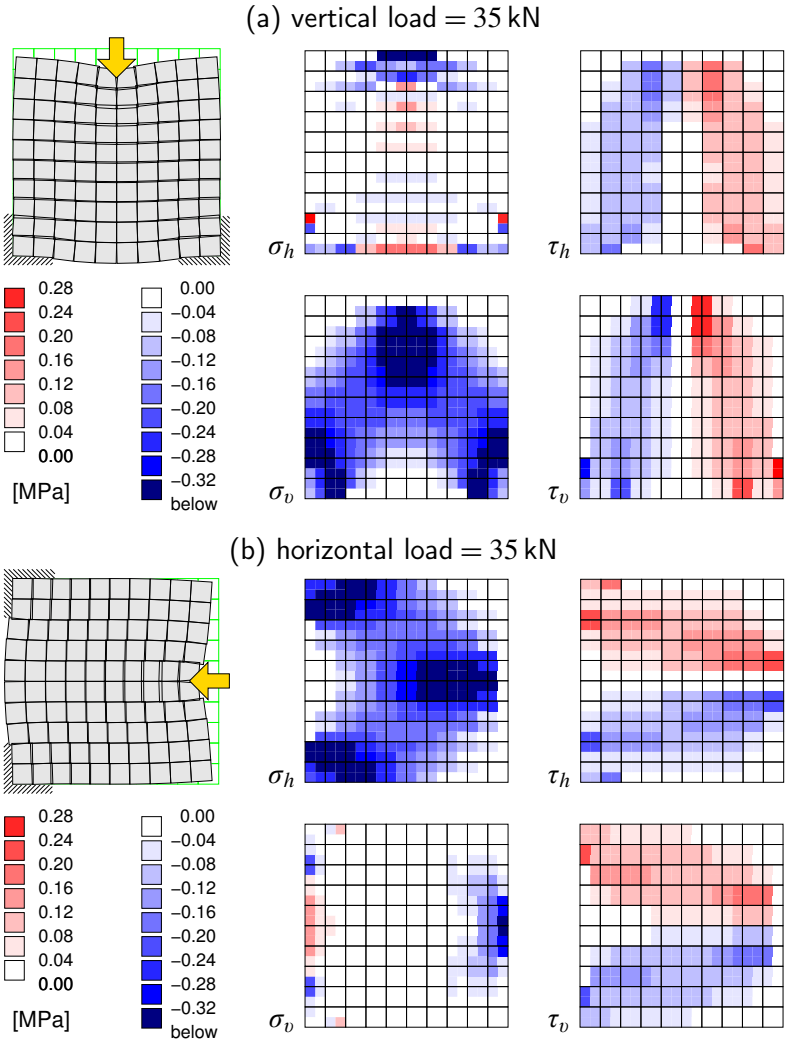

Figure 12. Deformed shape and maps of the generalised stresses in the axial springs (σ_h, σ_v) and in the shear springs (τ_h, τ_v) as obtained by means of the nonlinear rigid element model subjected to a vertical load (a) and a horizontal load (b).

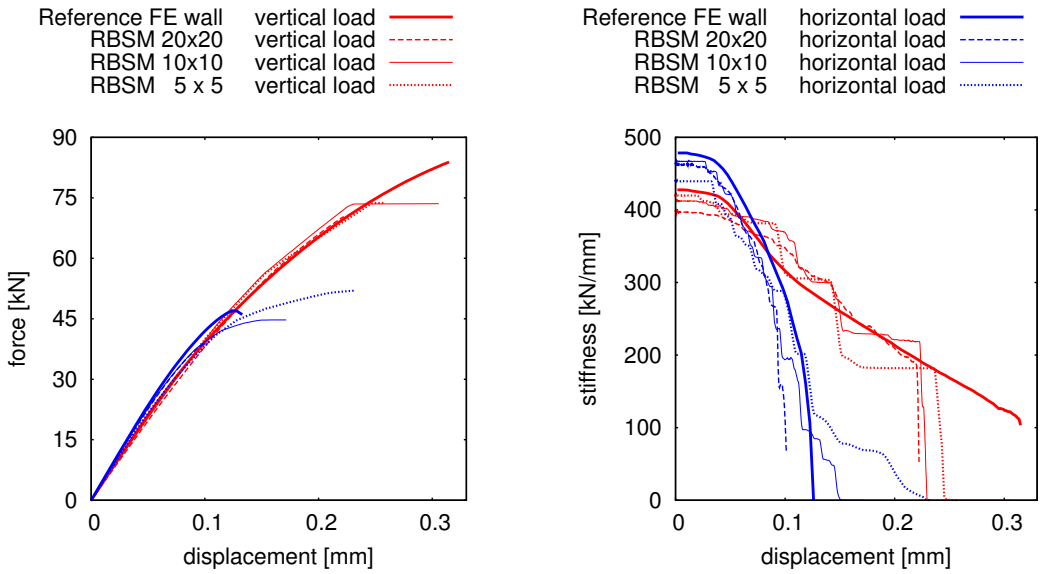

Figure 13. Force-displacement response curve and stiffness decay. The displacements are evaluated as the average in the loaded area.

maps it is also evident that the orthotropy of the shear springs favours the bearing capacity in the case of a vertical load, in conjugation with the presence of a prevailing situation of vertical compression stress.

The RBSM responses in terms of global variables are compared with the reference FE models in the graphs of Figure 13, where the results obtained with three different mesh refinements are shown together. The force-displacements curves are given on the left side, for both vertical (red lines) and horizontal (blue lines) loads. The corresponding curves of decay of the global stiffnesses are plotted on the right side Figure 13. They are evaluated by calculating the average slope of the previous curves. Globally, the performance can be judged as quite good, with the exception of the small underestimation of the bearing capacity in the vertical loading case.[7] The responses in terms of force show an acceptable sensitivity to the mesh size, being in the range 70.4–74.6 kN for the vertical load, and in the range 40.0–51.9 kN for the horizontal load. Note that the lower values are obtained with the finest mesh, for which there is a clear problem of localisation due to the fact that the element size is too small with respect to the internal characteristic length of the periodic material. The responses in terms of varying stiffness show the more pronounced stepped decay of the coarse meshes. It is worth noting that the RBSM is able to predict the very different bearing capacity of the two loading cases, as well as the completely different kinematics of the two collapse mechanisms, as shown in the enlarged detail of Figure 14. This capability is essentially related with the specific nonsymmetric characteristics of the shear springs and with the choice of adopting couples of axial springs placed at distances $b_x \neq b_y$. As a counter-check, when adopting a RBSM that does not have the present specific microstructure characteristics (i.e., the shear springs are symmetric and $\beta_x = \beta_y = 1/\sqrt{3}$), then the maximum loads are ~ 40 kN and ~ 45 kN for the vertical and horizontal

[7] In this connection, it is possible to enhance the model by introducing a specific rule for varying β_x as a function of the increasing damage. This would be in accord with the results obtained in [Casolo 2006], because β_x tends to increase as a function of the ratio between the elastic modulus of the blocks and of the mortar, while β_y tends to remain constant.

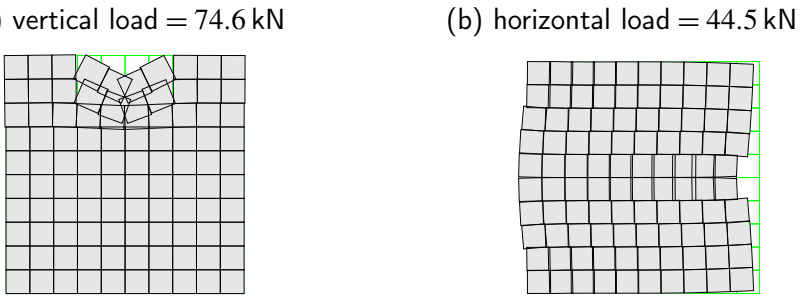

Figure 14. Enlarged detail of the collapse kinematics in the load application area with the 10×10 mesh.

loads respectively (note that in this case the vertical maximum load would be completely wrong, and even smaller than the horizontal). This performance seems particularly interesting when considering the results obtained with the coarsest mesh, for which a single element has the same size of the composite RVE.

3.3. ***Effects of mesh distortion on the RBSM.*** As already stated, each type of spring is associated almost exclusively with a definite damage pattern. Thus, the heuristic molecules should be regular, and as much as possible aligned in accord with the principal axes of the material texture, in order to grant a good performance. On the other hand, realistic applications sometimes require dealing with irregular geometries, even if a masonry-like material is usually laid down with a certain degree of regularity due to the presence of the horizontal mortar layers. In the linear-elastic case, this issue has already been considered in [Casolo 2004].[8] Now, the points that define the skeleton curve of an inclined spring must also be recalculated in order to account for the strength orthotropy. Given the couple of strengths ($\hat{\sigma}_v$ and $\hat{\sigma}_h$), along the vertical and horizontal directions, the most simple trigonometric rule has been chosen for evaluating the strength along a direction of inclination α: $\hat{\sigma}(\alpha) = \hat{\sigma}_h \cos^2\alpha + \hat{\sigma}_v \sin^2\alpha$. The performance of the RBSM has been tested by means of the meshes shown in Figure 15. The mesh on the right side has been named the bad mesh because of the high distortion of some elements, that are close to being triangles.

These meshes have been subjected to the same loading conditions described in the previous section, and Figure 16 shows graphs that compare the corresponding responses. It is evident that the performance can be judged as acceptable in the case of a limited distortion, while the bad mesh suffers for some problems of numerical convergence. It also tends to underestimate the bearing capacity of the reference wall in both situations.

[8] Given the angle of inclination α, the following expressions are adopted for the normal spring stiffness k^P and shear spring stiffness k^Q:

$$k^P(\alpha) = k_x^P \cos^4\alpha + k_y^P \sin^4\alpha + 4\frac{k_v^Q k_h^Q}{k_v^Q + k_h^Q}\cos^2\alpha \sin^2\alpha, \quad k^Q(\alpha) = \frac{2(k_x^P + k_y^P)\cos^2\alpha \sin^2\alpha + 2\frac{k_v^Q k_h^Q}{k_v^Q + k_h^Q}(\cos^2\alpha - \sin^2\alpha)^2}{1 - \frac{k_v^Q - k_h^Q}{k_v^Q + k_h^Q}(\cos^2\alpha - \sin^2\alpha)}.$$

Moreover we take $\beta(\alpha) = \beta_x \cos^2\alpha + \beta_y \sin^2\alpha$.

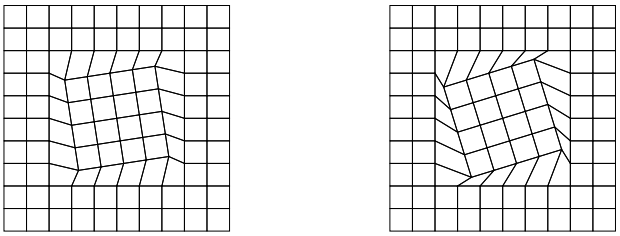

Figure 15. Meshes adopted to test the response in the case of geometric distortion. The reasonable (left) and the bad (right) meshes.

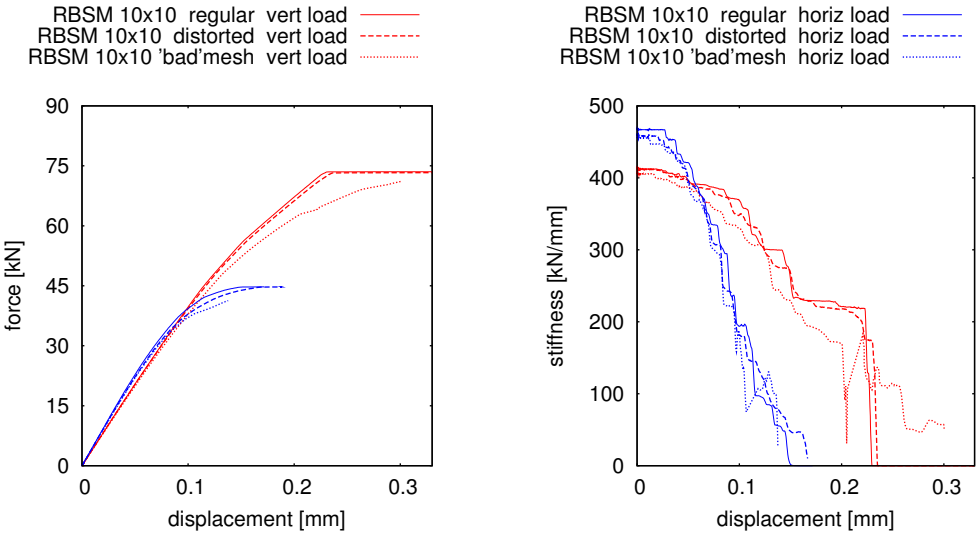

Figure 16. Comparison of the force-displacement response curve and stiffness decay when adopting distorted meshes.

4. Final remarks

The present contribution is part of a research project that has the objective of modelling the nonlinear response of masonry-like materials by a macroscale mechanistic approach. The core of the proposed rigid body and spring model (RBSM) is a specific heuristic molecule, or representative macroscopic segment made by four rigid elements, which has the capability of describing the fundamental damage mechanisms at the mesoscale, also including some mechanical effects that are strictly related with the internal microstructure. The parameters that govern the model can be obtained by relatively simple tests that consider the macroscale response of a RVE of the original microstructured material. The computer tests gave good results, in particular when considering the terrific reduction of the required degrees of freedom. At present, the idea is implemented into a specific Fortran computer code that has its natural engineering application in the field of the dynamics of structures made by complex nonlinear materials, as in the case of the seismic analysis of masonry monuments.

Appendix A: Matrix [B] for the case of square elements

The geometric strain-displacement relationship for the representative macroscopic segment, also called the heuristic molecule, is reported as an example (see Figure 17):

$$\begin{Bmatrix} \varepsilon_1^P \\ \varepsilon_1^Q \\ \varepsilon_1^R \\ \varepsilon_2^P \\ \varepsilon_2^Q \\ \varepsilon_2^R \\ \varepsilon_3^P \\ \varepsilon_3^Q \\ \varepsilon_3^R \\ \varepsilon_4^P \\ \varepsilon_4^Q \\ \varepsilon_4^R \end{Bmatrix} = \frac{1}{2e} \begin{bmatrix} 0 & 1 & -b & 0 & 0 & 0 & 0 & -1 & b & 0 & 0 & 0 \\ -1 & 0 & -e & 0 & 0 & 0 & 1 & 0 & -e & 0 & 0 & 0 \\ 0 & 1 & b & 0 & 0 & 0 & 0 & -1 & -b & 0 & 0 & 0 \\ -1 & 0 & -b & 1 & 0 & b & 0 & 0 & 0 & 0 & 0 & 0 \\ 0 & -1 & -e & 0 & 1 & -e & 0 & 0 & 0 & 0 & 0 & 0 \\ -1 & 0 & b & 1 & 0 & -b & 0 & 0 & 0 & 0 & 0 & 0 \\ 0 & 0 & 0 & 0 & 1 & -b & 0 & 0 & 0 & 0 & -1 & b \\ 0 & 0 & 0 & -1 & 0 & -e & 0 & 0 & 0 & 1 & 0 & -e \\ 0 & 0 & 0 & 0 & 1 & b & 0 & 0 & 0 & 0 & -1 & -b \\ 0 & 0 & 0 & 0 & 0 & 0 & -1 & 0 & -b & 1 & 0 & b \\ 0 & 0 & 0 & 0 & 0 & 0 & 0 & -1 & -e & 0 & 1 & -e \\ 0 & 0 & 0 & 0 & 0 & 0 & -1 & 0 & b & 1 & 0 & -b \end{bmatrix} \begin{Bmatrix} u_1 \\ v_1 \\ \psi_1 \\ u_2 \\ v_2 \\ \psi_2 \\ u_3 \\ v_3 \\ \psi_3 \\ u_4 \\ v_4 \\ \psi_4 \end{Bmatrix}.$$

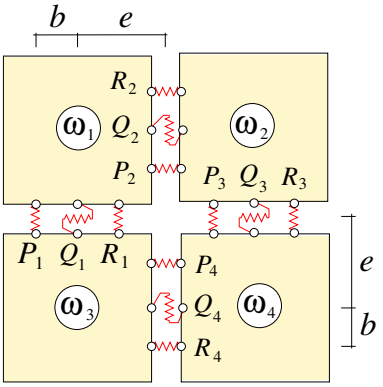

Figure 17. Example of a regular representative macroscopic segment, also referred to as a heuristic molecule.

Appendix B: Relationship with Cosserat continuum elastic moduli

Given the macroscopic axial elastic moduli $\mathsf{C}_{\alpha\alpha\beta\beta}$ that can be evaluated by applying antiperiodic tractions under symmetric periodic boundary conditions [Anthoine 1995], the stiffnesses per unit volume of the axial springs are:

$$k_x^P = k_x^R = \frac{\mathsf{C}_{1111}\mathsf{C}_{2222} - \mathsf{C}_{1122}^2}{\mathsf{C}_{2222}}, \qquad k_y^P = k_y^R = \frac{\mathsf{C}_{1111}\mathsf{C}_{2222} - \mathsf{C}_{1122}^2}{\mathsf{C}_{1111}}.$$

The stiffnesses of the orthotropic shear springs have the following relationship with the macroscopic Cosserat shear moduli C_{1212}, C_{1221}, and C_{2121}, in accordance with [Casolo 2006]:

$$k_h^Q = \frac{\mathsf{C}_{1212}\mathsf{C}_{2121} - \mathsf{C}_{1221}^2}{\mathsf{C}_{2121} - \mathsf{C}_{1221}}, \qquad k_v^Q = \frac{\mathsf{C}_{1212}\mathsf{C}_{2121} - \mathsf{C}_{1221}^2}{\mathsf{C}_{1212} - \mathsf{C}_{1221}}.$$

Finally, the distances b_x and b_y can be obtained as a function of the in-plane Cosserat flexural stiffnesses as follows [Casolo 2006]:

$$b_x = \beta_x e = \sqrt{\frac{\mathsf{D}_{3131}}{k_x^P}}, \qquad b_y = \beta_y e = \sqrt{\frac{\mathsf{D}_{3232}}{k_y^P}}.$$

References

[ABAQUS 2007] ABAQUS, *Abaqus documentation*, Version 6.7, Dassault Systèmes/SIMULIA, Providence, RI, 2007.

[Anthoine 1995] A. Anthoine, "Derivation of the in-plane elastic characteristics of masonry through homogenization theory", *Int. J. Solids Struct.* **32**:2 (1995), 137–163.

[Anthoine et al. 1995] A. Anthoine, G. Magenes, and G. Magonette, "Shear compression testing and analysis of brick masonry walls", pp. 1657–1662 in *Proceeding of the 10th European Conference on Earthquake Engineering* (Vienna, 1994), edited by G. Duma, A. A. Balkema, Rotterdam, 1995.

[Binda et al. 1992] L. Binda, G. Gatti, G. Mangano, C. Poggi, and G. Sacchi Landriani, "The collapse of the civic tower of Pavia: a survey of the materials and structure", *Masonry Int.* **6**:1 (1992), 11–20.

[Boffi and Casolo 1998] G. Boffi and S. Casolo, "Non-linear dynamic analysis of masonry arches", pp. 99–108 in *Monument 98: Workshop on Seismic Performance of Monuments* (Lisbon, 1998), Laboratório Nacional de Engenharia Civil, Lisbon, 1998.

[de Borst 2001] R. de Borst, "Some recent issues in computational failure mechanics", *Int. J. Numer. Methods Eng.* **52**:1 (2001), 63–95.

[Brasile et al. 2007] S. Brasile, R. Casciaro, and G. Formica, "Multilevel approach for brick masonry walls, I: A numerical strategy for the nonlinear analysis", *Comput. Methods Appl. Mech. Eng.* **196**:49–52 (2007), 4934–4951.

[Casolo 2000] S. Casolo, "Modelling the out-of-plane seismic behaviour of masonry walls by rigid elements", *Earthquake Eng. Struct. Dyn.* **29**:12 (2000), 1797–1813.

[Casolo 2004] S. Casolo, "Modelling in-plane micro-structure of masonry walls by rigid elements", *Int. J. Solids Struct.* **41**:13 (2004), 3625–3641.

[Casolo 2006] S. Casolo, "Macroscopic modelling of structured materials: relationship between orthotropic Cosserat continuum and rigid elements", *Int. J. Solids Struct.* **43**:3–4 (2006), 475–496.

[Casolo and Peña 2007] S. Casolo and F. Peña, "Rigid element model for in-plane dynamics of masonry walls considering hysteretic behaviour and damage", *Earthquake Eng. Struct. Dyn.* **36**:8 (2007), 1029–1048.

[Dhanasekar et al. 1985] M. Dhanasekar, A. W. Page, and P. W. Kleeman, "The failure of brick masonry under biaxial stresses", pp. 295–313 in *Proceedings of the Institution of Civil Engineers, 2: Research and theory*, vol. 79, Thomas Telford, London, 1985.

[Forest and Sab 1998] S. Forest and K. Sab, "Cosserat overall modeling of heterogeneous materials", *Mech. Res. Commun.* **25**:4 (1998), 449–454.

[Griffiths and Mustoe 2001] D. V. Griffiths and G. G. W. Mustoe, "Modelling of elastic continua using a grillage of structural elements based on discrete element concepts", *Int. J. Numer. Methods Eng.* **50**:7 (2001), 1759–1775.

[Kawai 1978] T. Kawai, "New discrete models and their application to seismic response analysis of structures", *Nucl. Eng. Des.* **48**:1 (1978), 207–229.

[Lemos 2007] J. V. Lemos, "Discrete element modeling of masonry structures", *Int. J. Archit. Herit.* **1**:2 (2007), 190–213.

[Lourénço et al. 1997] P. Lourénço, R. de Borst, and J. Rots, "A plane stress softening plasticity model for orthotropic materials", *Int. J. Numer. Methods Eng.* **40**:21 (1997), 4033–4057.

[Magenes and Calvi 1992] G. Magenes and G. M. Calvi, "Cyclic behaviour of brick masonry walls", pp. 3517–3522 in *Proceedings of the 10th World Conference on Earthquake Engineering* (Madrid, 1992), edited by A. Bernal, A. A. Balkema, Rotterdam, 1992.

[Malyszko 2005] L. Malyszko, "In-plane shear and tensile strength tests of small brickwork specimens", pp. 291–298 in *Structural analysis of historical constructions: possibilities of numerical and experimental techniques* (Padova, 2004), edited by C. Modena et al., A. A. Balkema, Leiden, 2005.

[Masiani et al. 1995] R. Masiani, N. Rizzi, and P. Trovalusci, "Masonry as structured continuum", *Meccanica* (*Milano*) **30**:6 (1995), 673–683.

[Massart et al. 2004] T. J. Massart, R. H. J. Peerlings, and M. G. D. Geers, "Mesoscopic modeling of failure and damage-induced anisotropy in brick masonry", *Eur. J. Mech. A Solids* **23**:5 (2004), 719–735.

[Milani et al. 2006] G. Milani, P. B. Lourenço, and A. Tralli, "Homogenised limit analysis of masonry walls, I: Failure surfaces", *Comput. Struct.* **84**:3–4 (2006), 166–180.

[Naraine and Sinha 1991] K. Naraine and S. Sinha, "Cyclic behavior of brick masonry under biaxial compression", *J. Struct. Eng.* (*ASCE*) **117**:5 (1991), 1336–1355.

[Ostoja-Starzewski 2002] M. Ostoja-Starzewski, "Lattice models in micromechanics", *Appl. Mech. Rev.* (*ASME*) **55**:1 (2002), 35–60.

[Pietruszczak and Ushaksaraei 2003] S. Pietruszczak and R. Ushaksaraei, "Description of inelastic behaviour of structural masonry", *Int. J. Solids Struct.* **40**:15 (2003), 4003–4019.

[Stakgold 1950] I. Stakgold, "The Cauchy relations in a molecular theory of elasticity", *Quart. Appl. Math.* **8**:2 (1950), 169–186.

[Sulem and Mühlhaus 1997] J. Sulem and H.-B. Mühlhaus, "A continuum model for periodic two-dimensional block structures", *Mech. Cohes. Frict. Mater.* **2**:1 (1997), 31–46.

[Trovalusci and Masiani 2005] P. Trovalusci and R. Masiani, "A multifield model for blocky materials based on multiscale description", *Int. J. Solids Struct.* **42**:21–22 (2005), 5778–5794.

[Zienkiewicz and Taylor 1991] O. C. Zienkiewicz and R. L. Taylor, *The finite element method*, vol. II, McGraw-Hill, London, 1991.

[Zucchini and Lourénço 2002] A. Zucchini and P. B. Lourénço, "A micro-mechanical model for the homogenisation of masonry", *Int. J. Solids Struct.* **39**:12 (2002), 3233–3255.

Received 31 Oct 2008. Revised 10 Feb 2009. Accepted 25 Feb 2009.

SIRO CASOLO: Siro.Casolo@polimi.it
Dipartimento di Ingegneria Strutturale, Politecnico di Milano, Piazza Leonardo da Vinci 32, 20133 Milano, Italy
http://www.stru.polimi.it/people/casolo/index.plp